

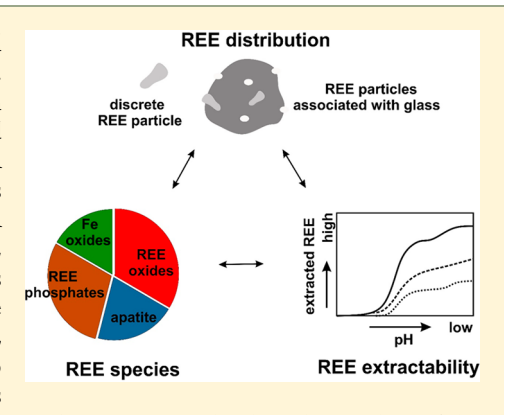
# Comprehensive Understandings of Rare Earth Element (REE) Speciation in Coal Fly Ashes and Implication for REE Extractability

Pan Liu, Rixiang Huang, and Yuanzhi Tang\*

School of Earth and Atmospheric Sciences, Georgia Institute of Technology, 311 Ferst Dr., Atlanta, Georgia 30332-0340, United States

Supporting Information

ABSTRACT: In recent years, recovery of rare earth elements (REEs) from coal fly ashes (CFAs) has been considered as a promising resource recovery option. Yet, quantitative information on REE speciation in CFAs and its correlation with REE extractability are not well established. This study systematically investigated the REE speciation-extractability relationship in four representative CFA samples by employing multiple analytical and spectroscopic techniques across the micro to bulk scale and in combination with thermodynamic calculations. A range of REE-bearing phases are identified, such as REE oxides, REE phosphates, apatite, zircon, and REE-bearing glass phase. REEs can occur as discrete particles, as particles encapsulated in the glass phase, or distribute throughout the glass phase. Although certain discrepancies exist on the REE speciation quantified by X-ray adsorption spectroscopy and acid leaching due to intrinsic limitations of each method, both approaches show significant fractions



of REE oxides, REE phosphates, apatite, and REE-bearing Fe oxides. This study contributes to an in-depth understanding of the REE speciation—distribution—extractability relationship in CFAs and can help identify uncertainties associated with the quantification of REE speciation. It also provides a general methodology for future studies on REE speciation in complex environmental samples and a knowledge basis for the development of effective REE recovery techniques.

## **■** INTRODUCTION

Rare earth elements (including lanthanides and yttrium, referred to as REEs hereafter) are critical for a wide range of high tech applications due to their unique physicochemical properties.1 The growing importance of REEs to technologies and economies and the potential risks of supply disruptions have led both the United States (US) and the European Union to label REEs as "critical materials". 2,3 The US is currently a net importer of REEs and spent \$150 million importing REEs in 2017.4 Over the recent years, there is great interest in developing economically feasible and environmentally friendly approaches for domestic REE recovery. 5-7 With this regard, coal combustion products, such as coal fly ashes (CFAs), have recently emerged as a promising REE source. 8-11 In the US, around 45 Mt CFAs are generated annually, with only 39% beneficially used and the rest discarded. 12 On the other hand, REEs are enriched in the CFAs after coal burning. 8,13 With an average total concentration of REE in CFAs at ~500 ppm, and the annual value of REEs derived from CFAs is estimated to be \$4.3 billion in the US. 10 Thus, recovery of REEs from CFAs is a promising waste recycling option that might bring about significant environmental, economic, and societal benefits.

In order to develop cost-effective and environmental friendly REE recovery techniques, many critical issues need to be addressed, including the following two fundamental questions, (1) the speciation of REEs in CFAs, such as the chemical species and physical distribution and/or association with other

phases, and (2) the controlling factors on REE extractability. Several previous studies <sup>14–16</sup> have suggested that REEs are dispersed throughout the amorphous aluminosilicate glass phase, thus the glass fraction should be targeted for REE recovery from CFAs. Other studies suggested the (predominant) presence of REEs in phosphate (e.g., monazite), <sup>17</sup> carbonate, <sup>18</sup> and/or silicate minerals (e.g., zircon). <sup>15</sup> Such inconsistency might result from the intrinsic heterogeneity of CFAs as well as the limitations of individual analytical methods.

Both micro- and bulk-scale analytical methods have been utilized to study the correlation between REE speciation (e.g., chemical species and physical distribution) and extractability in environmental samples, including CFAs. The main techniques used to study REE speciation include scanning/transmission electron microscopy coupled with energy dispersive X-ray spectroscopy (S/TEM-EDX), 15,17-19 electron probe microanalysis (EPMA), 19 laser ablation inductively coupled plasma mass spectrometry (ICP-MS), 15,20 and synchrotron X-ray microscopy and spectroscopy. Extractability evaluations were mainly conducted using sequential chemical extraction 23-25 and acid leaching. Although these techniques can

Received: January 2, 2019 Revised: March 25, 2019 Accepted: March 26, 2019 Published: March 26, 2019



Table 1. Chemical Characteristics of CFA Samples in This Study<sup>a,b</sup>

			major elements (wt %)			rare earth elements (ppm)			
sample	CFA type	coal source	SiO <sub>2</sub>	$Al_2O_3$	$Fe_2O_3$	CaO	Y	Nd	total
F-1	Class F	IL	54.3	25.2	11.9	1.6	$52.75 \pm 2.60$	$49.32 \pm 0.22$	$315.4 \pm 9.9$
F-2	Class F	surface mine in Craig, Co	55.3	23.3	5.1	8.0	$43.56 \pm 1.83$	$42.44 \pm 0.63$	$264.8 \pm 1.0$
C-1	Class C	PRB	36.6	18.2	6.4	28.1	$44.07 \pm 1.61$	$49.50 \pm 0.31$	$319.8 \pm 2.1$
C-2	Class C	PRB	36.0	18.5	6.3	25.8	$35.88 \pm 1.96$	$38.89 \pm 0.31$	$254.1 \pm 2.9$

<sup>a</sup>IL, Illinois basin; PRB, Powder River basin. Standard deviation was calculated based on three replicates. See Table S1 for more information. <sup>b</sup>Note: Major element information is from ref 28 (for samples F-1 and C-1) and NIST certificates (for samples F-2 and C-2).

provide valuable information (e.g., REE species, distribution, and extractability) at different spatial/temporal scales, they also possess intrinsic limitations. For example, direct information on REE extractability can be provided by sequential chemical extraction, but interpretation of the related mineral phases might be problematic, because this empirical method might cause incomplete dissolution of the desired phases, concomitant dissolution of different phases, or alteration of the original phases. To obtain a more complete picture and quantitative information on the REE speciation in complex matrices, such as CFAs, comparison and cross-validation of information obtained by different techniques are highly desired.

The goals of this study are to comprehensively characterize and quantify REE species and distribution in CFAs using complementary techniques across different spatial scales and to correlate the speciation information with REE extractability. Four representative CFA samples were selected by taking into consideration both the CFA chemical composition and main coal basins in the US. A systematic method was developed by employing techniques across the bulk to molecular scales, including chemical (acid leaching and sequential extraction), mineralogical (X-ray diffraction (XRD)), microscopic (SEM-EDX and synchrotron X-ray microscopy), and spectroscopic methods (synchrotron X-ray adsorption spectroscopy). On the basis of the results obtained, the advantages and disadvantages of each technique and controlling factors on REE extractability were evaluated. The results contribute to an improved understanding of REE occurrence in CFAs and their extractability, evaluate a general methodology for characterizing REE speciation in complex environmental matrices, and provide a knowledge basis for the development of cost-effective and environmentally friendly REE recovery methods.

#### MATERIALS AND METHODS

Materials. The American Society for Testing and Materials (ASTM) C 618 defines two classes of CFAs based on chemical characterization, Class F CFAs (with SiO<sub>2</sub> + Al<sub>2</sub>O<sub>3</sub> + Fe<sub>2</sub>O<sub>3</sub> ≥ 70 wt %) and Class C CFAs (with 50 wt %  $\leq$  SiO<sub>2</sub> + Al<sub>2</sub>O<sub>3</sub> +  $Fe_2O_3 \le 70$  wt %).<sup>27</sup> On the basis of this classification and the major coal basins in the US, four representative CFA samples were selected for this study (Table 1), including two CFA samples (F-1 and C-1) from a local coal-fired power plant located in the southeastern US<sup>28</sup> and two CFA samples from the National Institute of Standards and Technology (NIST) (SRM-2690 as F-2 and SRM-2691 as C-2 hereinafter). Samples F-1 and F-2 are Class F CFAs, and their feed coals are bituminous coal from the Illinois Basin and sub-bituminous coal from a surface mine in Craig, CO, respectively. Samples C-1 and C-2 are Class C CFAs, and their feed coals are subbituminous coals from the Powder River Basin (details in the Supporting Information, SI, Table S1). A suite of REE reference compounds (REE-organic complexes, REE oxides,

REE carbonates, REE phosphates, and natural REE-bearing minerals, etc.) were obtained or synthesized using chemicals of ACS grade or higher (details in Table S2). The synthesized and natural REE reference compounds were confirmed by XRD to be pure phases.

Composition Analysis and Chemical Extraction of REE in CFAs. REE contents in CFAs were determined from total digestion.<sup>29</sup> Two types of chemical extraction methods were used to assess the extractability of REEs, including sequential extraction and acid leaching. Sequential extraction was conducted following a previous procedure.<sup>30</sup> Briefly, four REE fractions were defined, (1) acid-soluble (step-1, e.g., carbonates), (2) reducible (step-2, e.g., Fe-Mn oxides), (3) oxidizable (step-3, e.g., organic matter and sulfide), and (4) residue (e.g., silicates). For acid leaching, REE extractability was investigated as a function of the pH being adjusted using HNO<sub>3</sub> and NaOH. At the desired pH, 0.2 g of CFAs per 100 mL of H<sub>2</sub>O was reacted for 3 days under agitations at room temperature. At the end of each chemical extraction step or acid leaching, REE concentration was analyzed using ICP-MS. Details on total digestion, sequential extraction, and ICP-MS measurement are in the SI, Text S1.

Mineralogical, Microscopic, and Spectroscopic Analysis of CFAs. XRD, SEM-EDX, micro X-ray fluorescence (μXRF) imaging and micro X-ray absorption near edge structure spectroscopy ( $\mu$ XANES), and bulk XANES analyses were conducted on the CFA samples. For XANES analyses, Nd and Y were chosen as representative light REEs (LREEs, from La to Sm) and heavy REEs (HREEs, from Eu to Lu plus Y), respectively.  $\mu$ XRF imaging and  $\mu$ XANES spectra of Y K-edge, Nd L<sub>III</sub>-edge, and Nd L<sub>II</sub>-edge were collected at Beamline 2-3 of the Stanford Synchrotron Radiation Lightsource (SSRL, Menlo Park, CA). Bulk XANES spectra were collected at Beamline 5-BM-D at the Advanced Photon Source (APS, Lemont, IL). Spectra of the reference compounds were also collected for liner combination fitting (LCF) analysis. Details on XRD, SEM-EDX, μXRF, and bulk/micro XANES data collection and LCF analysis are in the SI, Text S2.

# ■ RESULTS AND DISCUSSION

# Chemical and Mineralogical Characteristics of CFAs.

The element contents of CFA samples are listed in Tables 1 and S1 and compared to common CFAs from the major coal basins in the US. Samples F-1 and F-2 show a chemical composition typical of Class F CFAs that are enriched in SiO<sub>2</sub> (55%), Al<sub>2</sub>O<sub>3</sub> (25%), and Fe<sub>2</sub>O<sub>3</sub> (5–12%), while samples C-1 and C-2 as Class C CFAs are relatively depleted in the above elements but abundant in alkaline oxides (26–28% CaO and 1–5% MgO). Total REE content in Class F CFAs is similar to that of Class C CFAs (250–320 ppm), and comparable to common CFAs in the US (Table S1). REE patterns of the four CFA samples normalized (with subscript N) by the Upper

Continental Crust (UCC, representing the natural REE background)<sup>31</sup> are shown in Figure S1, which are in line with the general REE patterns of CFAs. REEs are M-type enriched  $(La_N/Sm_N < 1 \text{ and } Gd_N/Lu_N > 1)^8$  in both Class F and C CFAs without obvious Ce anomaly (defined as Ce\* = 2Ce<sub>N</sub>/(La<sub>N</sub> + Pr<sub>N</sub>)). Samples C-1, C-2, and F-2 are characterized with positive Eu anomaly (Eu\* = 2Eu<sub>N</sub>/(Sm<sub>N</sub> + Gd<sub>N</sub>)), while sample F-1 does not show evident anomaly.

The mineralogical composition of CFAs was investigated by XRD (Figure S2). Crystalline phases identified in Class F CFAs include quartz (SiO<sub>2</sub>), mullite (Al<sub>6</sub>Si<sub>2</sub>O<sub>13</sub>), hematite (Fe<sub>2</sub>O<sub>3</sub>), and magnetite (Fe<sub>3</sub>O<sub>4</sub>). Class C CFAs have a more complex mineralogy, with quartz, anhydrite (CaSO<sub>4</sub>), tricalcium aluminate (Ca<sub>3</sub>Al<sub>2</sub>O<sub>6</sub>), lime (CaO), and periclase (MgO) being identified. A broad hump at around  $20-30^{\circ}$   $2\theta$  suggests the presence of amorphous aluminosilicate glass, a common major component (50-80 wt %) in CFAs. 32 SEM analysis observed different morphologies of CFA particles, with the predominant presence of spherical and cenospherical particles ranging from 1 to 100  $\mu$ m (Figure S3). Such morphological features are typical for CFAs due to particle melting and decomposition during the coal burning process.<sup>33</sup> In addition, considerable amounts of fine particles (e.g., Fe oxides) were found to be embedded within the glass phase in both Class F and C CFAs (Figures S3 and S4).

REE Speciation by SEM-EDX. SEM-EDX observed two types of REE occurrences in CFAs, including pure REE phosphates and minor REEs in lime and zircon. Figure 1a shows an REE phosphate particle ( $\sim 30-\mu m$  size) that is enriched in LREEs, while the one in Figure 1b ( $\sim$ 10- $\mu$ m size) is enriched in HREEs with close association with the aluminosilicate glass. These two REE phosphate particles

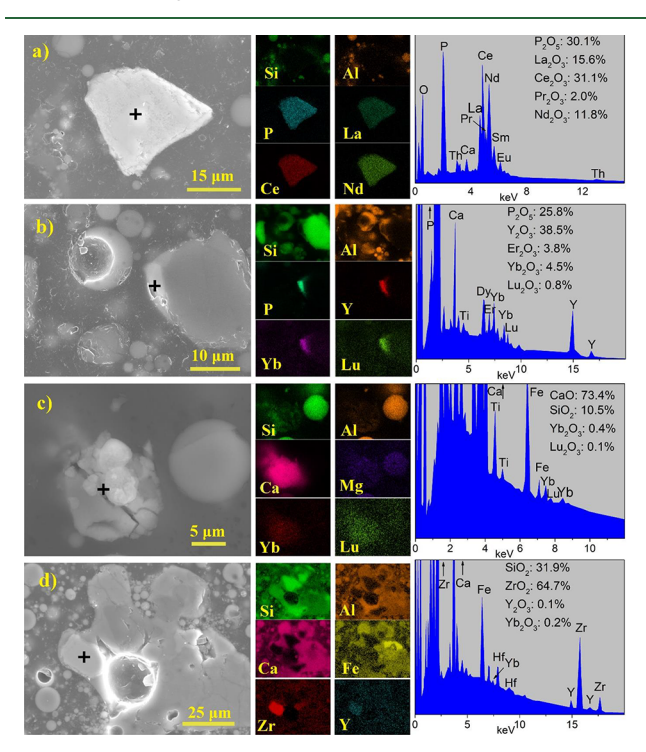


Figure 1. SEM images (left panels), EDX maps (middle small panels), and EDX spectra (right panels) showing REE-bearing phases in CFAs. (a) Monazite in sample F-1, (b) xenotime in sample F-2, (c) Ca-rich phase in sample C-1, and (d) zircon in sample C-1. Black crosses denote points for EDX measurements.

might be monazite/rhabdophane (LREE-enriched phosphate) and xenotime/churchite (HREE-enriched phosphate), respectively. Monazite and xenotime are anhydrous phosphate minerals, while rhabdophane and churchite are hydrated phosphate minerals. It is difficult to differentiate them by SEM-EDX. REE phosphates have also been identified previously using TEM<sup>17,34</sup> and EPMA.<sup>19</sup> A lime (CaO) particle containing minor REEs (REE oxide content < 0.5 wt %) is shown in Figure 1c. This phase contains minor HREEs, and its spherical shape suggests that it might be a relic of the REE-bearing CaCO<sub>3</sub> after burning. Both REE-bearing CaCO<sub>3</sub> and CaO have been previously identified. 18,19 A zircon (ZrSiO<sub>4</sub>) particle (REE oxide content < 0.3 wt %) is shown in Figure 1d, which is encapsulated in the glass phase. Although zircon is relatively abundant in the CFAs, only a portion of observed zircon particles (4 out of 16) contains EDX-detectable REEs. Other potential REE-bearing phases, such as apatite<sup>19</sup> and glass phase, 14 were observed but with no REEs detected by EDX.

An overview of the REE speciation observed by SEM-EDX reveals three critical features regarding REE occurrence in CFAs (Table S3). First, different phases might preferentially accommodate LREEs or HREEs. LREEs are more enriched in monazite/rhabdophane and HREEs in xenotime/churchite, lime, and zircon (Figure 1). This phenomenon might be due to the gradually decreasing cation radii of REEs with increasing atomic number (i.e., lanthanum contraction), which changes the compatibility of individual REE elements for a specific mineral phase. Second, as shown in Figures 1 and S5, REEbearing phases can occur as discrete particles or be closely associated with the glass phase (at the edge or totally encapsulated). The close association of REE-bearing phases with the glass phase is likely due to the capture of REE-bearing phases during glass cooling and agglomeration,<sup>21</sup> and it has also been noticed by several previous studies (e.g., refs 17,21). Third, REE-bearing phases might be subjected to decomposition during combustion. Although REE phosphates and zircon are typically thought to be stable, even at high temperature (e.g., ref 19), Figure S6 shows decomposition characteristics of REE phosphates (particle shattering) and zircon (holes and melting features), as compared to Figure 1a,d, respectively.

REE Speciation by Synchrotron Microscopy and **Spectroscopy.** Characteristics of REE Reference Compounds. Y XANES spectra of reference compounds are plotted in Figures S7. Spectra of Y<sub>2</sub>O<sub>3</sub>, Y-churchite (YPO<sub>4</sub>· H<sub>2</sub>O), apatite (Ca<sub>5</sub>(PO<sub>4</sub>)<sub>3</sub>(OH, F)), REE-bearing calcite (CaCO<sub>3</sub>), monazite ((Ce, Th, La, Nd)PO<sub>4</sub>), xenotime ((Y, Dy)PO<sub>4</sub>), zircon (ZrSiO<sub>4</sub>), and REE-bearing glass all show a peak at 17056.5 eV and a shoulder at 17066 eV, but the relative intensities are different and have additional features at 17080-17140 eV. These different spectral features reflect different structures and local coordination environments of the REE reference compounds (such as the first shell coordination, summarized in Table S2). On the other hand, Y spectra of  $Y^{3+}(aq)$ , Y-tengerite  $(Y_2(CO_3)_3 \cdot 2 - 3H_2O)$ , bastnäsite  $((Ce, La, Count)_3 \cdot 2 - 3H_2O)$ Nd)CO<sub>3</sub>(OH, F)), REE-bearing hematite (Fe<sub>2</sub>O<sub>3</sub>), and REEorganic complexes are similar to each other, showing a single peak at around 17056.5 eV, although the peak position is slightly right-shifted for Y<sup>3+</sup>(aq) and left-shifted for bastnäsite.

Nd spectra were not collected for some reference compounds (e.g., bastnäsite and monazite) due to interference of the Ce L<sub>II</sub>-edge signal on the Nd L<sub>III</sub>-edge and Sm L<sub>III</sub>-edge signal on the Nd  $L_{\rm II}$ -edge. For reference compounds with Nd spectra obtained, their  $L_{\rm III}$ - and  $L_{\rm II}$ -edge spectra are generally similar in appearance, with a characteristic intense main peak (Figure S8), making it difficult to distinguish REE speciation based on Nd XANES. Thus, Y was used as the primary "probe" for characterizing REE speciation. Although some Y spectra of the REE-reference compounds are similar, giving the possibility that some subtle differences might still be helpful in differentiating REE speciation, all 13 Y reference spectra were used for the linear combination fitting (LCF).

 $\mu$ XRF and  $\mu$ XANES Analyses. Representative  $\mu$ XRF maps are plotted in Figures 2, S9, and S10. Most Y hotspots

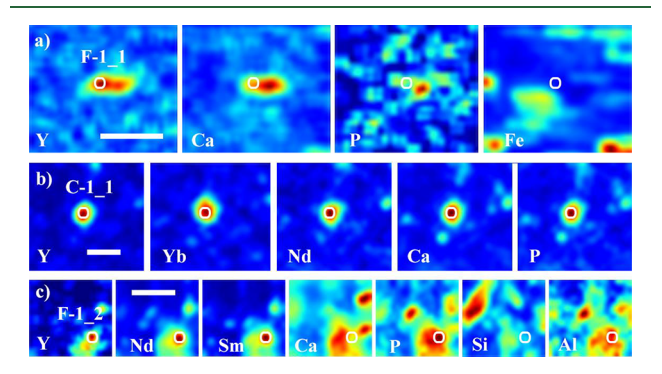


**Figure 2.** Representative synchrotron  $\mu$ XRF maps of selected REEs and major elements in CFAs. (a) Y, Ca, P, and Fe maps of sample F-1 collected at 17.2 keV. (b) Y (collected at 17.2 keV) and Yb, Nd, Ca, and P maps (collected at 10 keV) of sample C-1. (c) Y (collected at 17.2 keV) and Nd, Sm, Ca, P, Si, and Al maps (collected at 10 keV) of sample F-1. White scale bars represent 50  $\mu$ m. REE hotspots (indicated by white open circles) were selected for  $\mu$ XANES analysis.

observed have a particle size of  $<50 \mu m$  (Figure 2) and are colocalized with a range of elements, including Si, P, Ca, Fe, and

other REEs (Table S4). Y  $\mu$ XANES spectra were collected at Y hotspots and fitted using REE reference compounds (Figure 3). When Y was co-localized with other LREEs, Nd  $\mu$ XANES spectra were also collected to check the signal reality, giving the possible interference of other elements (e.g., Ba, Ti, and V). Element composition and distribution information based on  $\mu$ XRF and LCF results of Y  $\mu$ XANES (summarized in Table S4) were used to identify REE-bearing phases in CFAs, which is complementary to the SEM/EDX analysis.

Identified potential REE-bearing phases include apatite, REE phosphates, REE oxides, and REE-bearing glass phase. Hotspot F-1 1 (Figure 2a) is an example of apatite observed, of which Y is co-localized with Ca and P, and LCF suggests a significant fraction of apatite (48-72%). REE phosphates might be present at hotspots C-1 1 (Figure 2b) and F-1 3 and F-2 1 (Figure S9), characterized with discrete Y hotspots, colocalization of Y with other HREEs (e.g., Ho and Yb), and significant fractions of REE phosphates (>60%) at those hotspots by LCF. Five hotspots are identified as REE oxides (Table S4), and they have a relatively smaller particle size (generally  $<35 \mu m$ ) (Figures S9 and S10). Those hotspots can be fitted by 60-70% Y<sub>2</sub>O<sub>3</sub>, with the rest consisting of REE phosphates or REE carbonates. REE oxides in CFAs might result from the decomposition of REE phosphates and/or carbonates during combustion (i.e.,  $2YPO_4 \rightarrow Y_2O_3 + P_2O_5^2$ and  $Y_2(CO_3)_3 \rightarrow Y_2O_3 + 3CO_2$ ). At hotspot F-1\_2 (Figure 2c), Y and other REEs are distributed throughout an Caenriched aluminosilicate particle. Both collected Y and Nd uXANES are noisy, likely due to their low concentration in the glass phase. The co-localization of REEs with P and Ca in this glass phase suggests it might form through apatite decomposition and mixing with glass during combustion. REE speciation at hotspots C-1 2 and C-2 3 cannot be determined due to the limited  $\mu$ XRF information and no or indistinguishable LCF results.

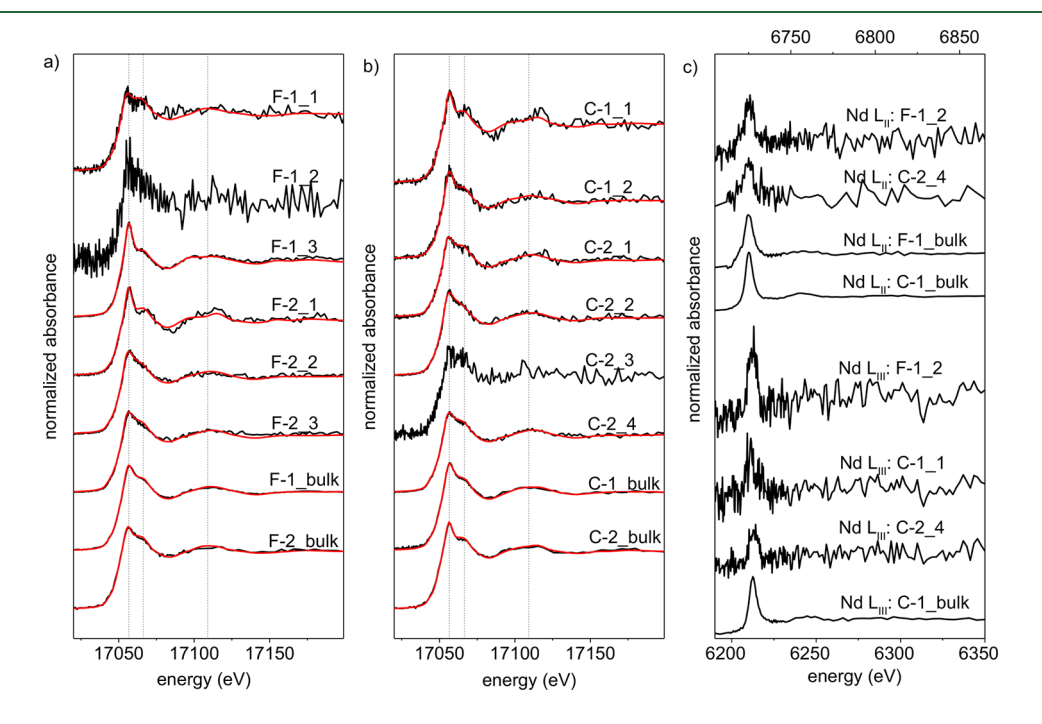
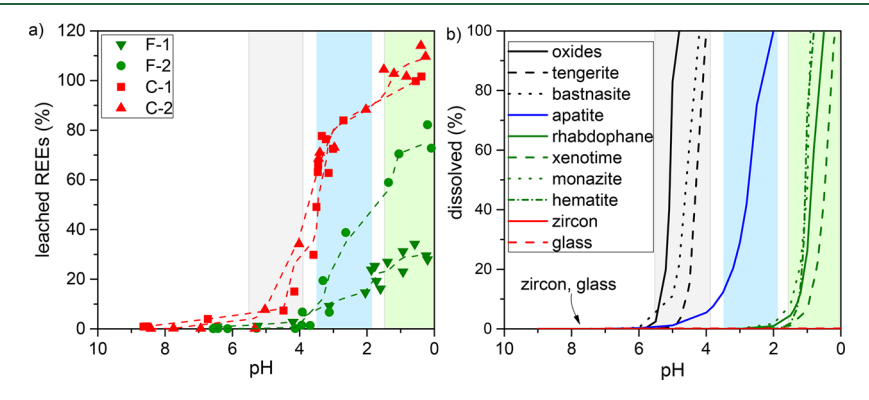


Figure 3. Y K-edge and Nd  $L_{II}$ - and  $L_{III}$ -edge XANES spectra (black lines) of CFAs, as well as LCF results (red lines) using REE reference compounds. (a) Y micro and bulk XANES of Class F CFAs. (b) Y micro and bulk XANES of Class C CFAs. (c) Nd  $L_{III}$ -edge and  $L_{III}$ -edge micro and bulk XANES of CFAs. The relative fractions of REE reference compounds by LCF are listed in Tables S4 and S5 (highlighted in blue).

Table 2. Summary of REE Speciation Fractions in CFAs Quantified by LCF of Y Bulk XANES and Acid Leaching

					acid leaching $(\%)^b$				
sample	LCF of Y bulk XANES (%) <sup>a</sup>			pH > 3.5 (REE oxides, carbonates)	pH 3.5-1.5 (apatite)	pH < 1.5 (REE phosphates, hematite)	residue (glass, zircon)		
F-1	norm		Y-churchite, $24.8 \pm 3.1$	hematite, $19.1 \pm 2.8$	~10	~10	~10	~70	
	deriv		Y-churchite, $21.2 \pm 2.8$	hematite, $29.4 \pm 2.9$					
F-2	norm	$Y_2O_3$ , 43.7 ± 3.6	apatite, $36.2 \pm 5.6$	hematite, $18.0 \pm 3.6$	~10	~40	~20	~30	
	deriv	$Y_2O_3$ , 44.7 ± 7.1	apatite, $21.4 \pm 6.4$	hematite, $28.0 \pm 4.6$					
C-1	norm		xenotime, $20.2 \pm 3.3$	hematite, $29.4 \pm 2.9$	~50	~40	~10		
	deriv	$Y_2O_3,$ 43.2 ± 6.2	Y-churchite, $52.7 \pm 4.2$						
C-2	norm	$Y_2O_3, 34.4 \pm 2.9$	xenotime, $42.0 \pm 2.5$	apatite, $21.5 \pm 3.5$	~60	~30	~10		
	deriv	$Y_2O_3,$ $40.0 \pm 5.0$	monazite, $50.3 \pm 3.3$						

"LCF results listed here are fits with similar REE speciation and fit weights, obtained by fitting the normalized spectra (marked as norm) or the first derivatives (marked as deriv). See Text S2 for the LCF process, Table S2 for information on REE reference compounds used in LCF, and Table S5 for more results of combinational fits. "REE carbonates include tengerite and bastnäsite, while REE phosphates include rhabdophane, churchite, monazite, and xenotime. The quantification of REE fractions was based on the results from acid leaching experiments of CFAs conducted at different pHs and calculated dissolution curves and dissolution experiments of REE reference compounds. See Figures 4 and S12 and details in the REE Speciation and Extractability by Sequential Extraction and Acid Leaching section.



**Figure 4.** (a) Percentage of leached REEs from CFAs as a function of pH, with red and green colors representing Class C and F CFAs, respectively. (b) Percent dissolution of pure REE-bearing phases as a function of pH calculated by PHREEQC using published thermodynamic data. Dash line in (a) was plotted using the adjacent-averaging function. Dissolution of REE-bearing phases was calculated with 50 mg of solids in 100 mL of 0.1 M NaCl solution. See Table S2 for details of the thermodynamic data.

Bulk XANES Analysis. Y bulk XANES spectra of CFAs show a main peak at 17056.5 eV and a shoulder at around 17066 eV, and all Nd bulk XANES spectra display a single main peak (Figure 3). LCF was not conducted on Nd XANES due to the large spectral similarity, while both the normalized Y bulk XANES spectra and their first derivatives were fitted to quantify REE speciation in CFAs (Text S2). It is noticed, that some top fits were indistinguishable by the *R*-factor (i.e., with *R*-factor difference <10%) (Table S5), and thus, similar LCF results (i.e., similar REE speciation and fit weights) given by the two fitting approaches were regarded as the final LCF results (Table 2) and are discussed below.

For Class F CFAs, the main Y species are REE oxides (40–55%), REE-bearing hematite (20–30%), and REE phosphates (20–25%) or apatite (20–35%). On the other hand, Class C CFAs contain a significant fraction of REE oxides (35–50%) but with different fractions and combinations of other REE species. Indeed, it appears that LCF is unable to determine whether the remnant REEs in Class C CFAs occurs as a single REE phosphate mineral or as a combination of REE phosphate

mineral and REE-bearing hematite or apatite (Table 2). Such a limitation may be due to the data quality of the obtained Y XANES spectra, since Y is less concentrated in Class C CFAs than that in Class F CFAs (Table 1), and it may also result from the spectral similarity of REE reference compounds (Figure S7).

It is worth noting, that, regardless of CFA type and origins, there are significant amounts of REE oxides (35–55%) in CFAs. Considering that REEs rarely occur as oxides in coals, and such a dominant presence of REE oxides in CFAs might, again, suggest REE speciation transformation during combustion, such as the decomposition of REE phosphates or carbonates. For the other main REE species in the CFA samples, LCF shows the presence of REE phosphate, REE-bearing hematite, and apatite. Such an observation is slightly different from the results of a recent work using the LCF of Y XANES, which suggested the primary presence of REE oxides (18–51%) and REE-bearing glass (22–76%). Although REE-bearing glass might comprise up to 50% for some top fits (Table S5), it never appears both in the fits of the normalized

spectra and the derivatives. On the other hand, ref 22 only fitted the normalized spectra, and it might be necessary to also fit the derivatives to double check the presence and quantity of REE-bearing glass.

REE Speciation and Extractability by Sequential Extraction and Acid Leaching. In order to investigate REE extractability and validate the above obtained information on REE speciation, acid leaching of CFAs as a function of pH as well as sequential extraction were conducted. Both acid leaching and sequential extraction are chemical extraction methods. On the basis of our results, empirically defined sequential extraction results do not contribute more information than acid leaching. Therefore, the results and discussion in the main text are based on the acid leaching results to avoid redundancy, and the results from the sequential extraction are detailed in Text S3, Table S6, and Figure S11.

As shown in Figure 4a, decreasing the pH leads to the gradual increase of leached REEs for all four CFAs, but REE extractability of Class C CFAs (~100%) is higher than that of Class F CFAs (30-70%). Moreover, the gradual increase of leached REEs with decreasing pH displays three main stages at pH 5.5-3.5, 3.5-1.5, and <1.5 (Figure 4a), indicating a stepwise dissolution of REE-bearing phases. In order to confirm this hypothesis, dissolution of the REE reference compounds was calculated using the geochemical software PHREEQC<sup>35</sup> with solubility data compiled from literature (summarized in Table S2). As shown in Figure 4b, the dissolution of the REE reference compounds as a function of pH can be classified into four groups, (1) REE oxides and REE carbonates (tengerite and bastnäsite) dissolved at pH 5.5-4, (2) apatite dissolved at pH 3.5-2, (3) REE phosphates (rhabdophane, churchite, xenotime, and monazite) and hematite dissolved at pH < 1.5, and (4) zircon and glass phase barely dissolved under the tested pH range. To further validate the results from thermodynamic calculation, acid dissolution of the selected REE reference compounds was also conducted at pH 7, 4, and 1.5, and the results (Figure S12) are consistent with the calculation.

On the basis of the above observations, the first increase of acid-leached REEs from CFAs is likely associated with REE oxides and carbonates (pH 5.5-3.5), the second with apatite (pH 3.5-1.5), the third with REE phosphate and hematite (pH < 1.5), and the rest in the zircon and glass phase. On the basis of this, for sample F-1, 70% of REEs are estimated to be associated with the zircon and glass phase, 10% with REE oxides and carbonates, 10% with apatite, and 10% with REE phosphates and hematite (Table 2). However, for sample F-2, 30% of REEs are in the zircon and glass phase, with 40% in apatite, 20% as REE phosphates and hematite, and 10% as REE oxides and carbonates. In contrast, 50-60% of REEs in samples C-1 and C-2 are REE oxides and carbonates, with 20-30% in apatite and 20% as REE phosphates and hematite.

Comparative Analysis of Results from Different Techniques. A comparative analysis of our results obtained from different techniques is discussed below in order to obtain a more comprehensive understanding of REE speciation in CFAs and to identify any discrepancies and the causes.

REE Speciation and Distribution at Microscale. SEM-EDX is able to identify most REE-bearing phases with an REE content of >0.1 wt %, but apatite and REE-bearing glass are only identified by  $\mu$ XRF/ $\mu$ XANES, likely due to the difference in detection limits of these techniques. Meanwhile, REEbearing lime and zircon are not identified by  $\mu XRF/\mu XANES$ .

Lime might be interpreted as REE oxides using  $\mu XRF/$  $\mu$ XANES (e.g., hotspot F-2 3, of which Y is co-localized with Ca). Zircon is not observed because the excitation energy of 17.2 keV is below the Zr K-edge (18 keV). Except for these observations, REE speciation and their distributions observed by SEM-EDX and  $\mu$ XRF/ $\mu$ XANES are consistent. REEs in CFAs occur as REE oxides, REE phosphates, apatite, zircon, and the REE-bearing glass phase (Tables S3 and S4). As for REE distribution, REEs can occur as discrete particles (Figures 1a and 2a), as particles embedded in the glass phase (Figure 1b,d), or distribute throughout the glass phases (Figure 2c), which is in line with a recent study using  $\mu$ XRF and  $\mu$ XANES of Ce (ref 21). Additionally, REE-bearing phases can undergo varying degrees of decomposition during coal combustion, which was suggested by the morphological features (Figure S6) and LCF results (Table S4) as observed by SEM-EDX and  $\mu$ XANES, respectively.

REE Speciation and Extractability at Bulk Scale. The fractions of REE species in CFAs determined by LCF of Y XANES and acid leaching, however, do not completely correlate with each other (Table 2). For example, although both LCF and acid leaching suggest sample F-2 contains ~40% of REEs as apatite and ~20% of REEs as REE-bearing hematite, LCF suggests ~45% of REEs as REE oxides in sample F-2, while acid leaching suggests ~10% of REEs as REE oxides and carbonates and ~30% of REEs as zircon and the glass phase. Similarly, for samples C-1 and C-2, both the LCF and acid leaching suggest the significant fraction of REE oxides (35-60%) and the absence of zircon and the glass phase, but quantification of other REE speciation is different. For sample F-1, LCF and acid leaching provide totally different quantifications of REE speciation.

Such an observed discrepancy might be due to the following factors. On the one hand, challenges for LCF of XANES are present due to spectral similarity of different REE reference compounds. As noticed, some REE reference compounds could replace others (either individual spectrum or combinations of spectra) without significantly reducing the quality of fitting (see top fits of F-1 and F-2 in Table S5). In practice, it might be difficult to differentiate the third (or even the second) REE-bearing phase in CFAs depending on the XANES data quality. On the other hand, the close association of REE-bearing phases with the glass phase as observed by SEM-EDX (Figures 1 and S5) might prevent dissolution of REE species at the desired pH during acid leaching (or designated steps during sequential extraction). To confirm this, XRD analysis was conducted on the solids after acid leaching and each sequential extraction step. Indeed, certain phases, such as hematite and magnetite, do not totally dissolve at a desired extraction step/pH, likely due to the encapsulation of these phases by the glass phase (Figures S3 and S4). It might be the case for REE-bearing phases as well, resulting in underestimation of certain REE speciation (e.g., REE oxides, carbonates, apatite, etc.) and overestimation of the glass phase and zircon. For example, ~70% of REEs in Sample F-1 are estimated to be in the glass phase or zircon, which might be an

In summary, SEM-EDX and  $\mu$ XRF/ $\mu$ XANES are capable of identifying REE-bearing phases and displaying their distribution in CFAs, and they provide combined evidence that REEbearing phases might occur as discrete particles or be closely associated with the glass phase, with features suggesting varying degrees of chemical decomposition. Although the

Table 3. Summary and Comparison on the Advantages and Disadvantages of Different Methods for Identifying/Quantifying REE Speciation and Evaluating REE Extractability

methods	scale	information provided	limitation
SEM-EDX	micro	•Identification of REE-bearing phases	•Due to spatial resolution and/or detection limit, REE-bearing phases might be difficult to find
		Particle morphology and distribution	•Difficult to quantify REE species
$\mu$ XRF and $\mu$ XANES	micro	●Distribution of REEs at trace level ●Identification of REE-bearing phases	●No information on REE extractability
bulk XANES	bulk	•Average REE local structures (~5 Å) and oxidation states	●No direct information on REE species
		Quantification of REE-bearing phases by linear combination fitting	•No information on REE distribution
			•Quantification of REE-bearing phases might be problematic due to data quality and spectral similarities of reference compounds
			●No information on REE extractability
acid leaching and thermodynamic calculation	bulk	•Indirect information on REE fractions based on different solubilities of REE species as a function of pH	●No direct evidence of REE species
		•REE extractability	•No information on REE distribution
	1 11	The state of the period of	O of a family 1 that 11 of 1 of
sequential extraction	bulk	Indirect information on REE fractions from different extraction steps (reagent and pH)     REE extractability	<ul> <li>Quantification of REE-bearing phases might be problematic due to empirical interpretations, matrix effects, and alteration of REE-bearing phases during extraction</li> </ul>

fractions of REE speciation determined by the LCF of XANES and acid leaching do not completely correlate with each other, both methods show that the main REE speciation in CFAs includes REE oxides, apatite, REE-bearing Fe oxides, and REE phosphates. Compared to most previous studies on REE speciation and/or REE extractability without cross-validation using different methods, our combined results from SEM-EDX,  $\mu$ XRF/ $\mu$ XANES, bulk XANES, and acid leaching provide an in-depth evaluation of the REE speciation—distribution—extractability relationship in CFAs and can also help identify uncertainties associated with the quantification of REE speciation using different methods.

## **■** IMPLICATION

Methodology for Studying REE Speciation and Extractability in Complex Environmental Samples. With the growing interests in REE recovery/recycling from waste streams (e.g., CFAs, red mud, <sup>36</sup> and acid drainage <sup>37</sup>) and natural resources (e.g., deep sea mud <sup>38</sup> and Georgia kaolins <sup>39</sup>), it is necessary to develop a general methodology for studying REE speciation in those complex environmental samples. By comparing the results, advantages, and disadvantages of different techniques used in this study (Table 3), recommendations for future studies on REE speciation and extractability in environmental samples are summarized below.

Both SEM-EDX and  $\mu$ XRF/ $\mu$ XANES are powerful techniques for studying REE species and distribution in complex matrices, and  $\mu$ XRF/ $\mu$ XANES might be more suitable for environmental samples with a low-REE content. Additionally, attention should be paid to the physical distribution of REEs. Close association of REE-bearing phases with other major components might occur in environmental samples as well, such as association with organic matter and/or coating by clays or other organic/mineral substances. Thus, physical distribution of REEs in environmental samples should also be considered along with chemical species, since both would influence the apparent REE extractability.

LCF of XANES can be challenging to provide complete and quantitative information on REE speciation in CFAs, partly due to the intrinsic spectral similarity of different REE reference compounds. A brief review of XANES studies on REEs (e.g., refs 21,22,40,41) reveals that Y is the only element possessing a variety of XANES spectral features. Thus, future studies may still consider using Y as the primary "probe" to quantify REE speciation in environmental samples, but the results should be interpreted with caution and cross-validated with other techniques. In this study, a stepwise dissolution of REE reference compounds as a function of pH is established (Figure 4b), and future studies can consider using pH 3.5, 1.5, and 0 as the "critical pH values" for quantifying REE speciation in environmental samples and to validate the results from the LCF of XANES data. If the conventional sequential extraction method is used, we also provide recommended interpretations of REE speciation for each step (details in Table S6). However, one should keep in mind, that, depending on the particle size, crystallinity, and impurities of REE species in the samples, the dissolution curve as a function of pH might be either left- or right-shifted. Additionally, the physical distribution (e.g., encapsulation and coating) might also affect dissolution kinetics. Overall, the quantification of REE species in environmental samples is challenging and requires combined results from different techniques to identify uncertainty associated with each technique.

Implication for REE Recovery from CFAs. The U.S. Department of Energy (DOE) has launched several programs to develop cost-effective and environmentally friendly techniques for recovering REEs from coals and coal combustion products. Previous studies proposed that recovering REEs from CFAs should target the glass phase and use strong acids or alkalis at high temperature (e.g., refs 17,19,25,42), which might be adequate for sample F-1 (with a low-REE extractability). Physical separation might be applied to this type of sample to enrich REEs in related phases, such as size, magnetic, and density separations. On the other hand, sample F-2 and, more generally, Class C CFAs show higher

REE extractability (70–100%), due to the presence of REE oxides and apatite that can be readily processed (such as using pH-dependent separation or inorganic/organic ligands with a high affinity with REEs). Additionally, although LREEs and HREEs might be preferentially enriched in different phases (Figures 1, S5, and S6), they showed similar mobility during chemical extraction (Figure S11). It is well-known, that some inorganic/organic ligands (e.g., carboxylic acids<sup>44</sup>) have a higher affinity with HREEs than LREEs, which might be developed to selectively dissolve HREEs vs LREEs. Thus, future studies may further investigate the feasibility and optimization of REE recovery and separation using natural or engineered ligands under varied pH conditions.

### ASSOCIATED CONTENT

# **S** Supporting Information

The Supporting Information is available free of charge on the ACS Publications website at DOI: 10.1021/acs.est.9b00005.

Texts for total digestion, sequential extraction, and setup and data analysis of XRD-EDX, SEM, and XANES; tables for CFA compositions, REE reference compounds, results of SEM-EDX,  $\mu$ XRF/ $\mu$ XANES, bulk XANES, and sequential extraction; and plots for REE patterns of CFAs, XRD patterns, SEM-EDX images, XANES spectra of REE reference compounds,  $\mu$ XRF images, sequential extraction, and dissolution curve of REE reference compounds (PDF)

#### AUTHOR INFORMATION

# **Corresponding Author**

\*Email: yuanzhi.tang@eas.gatech.edu; Phone: 404-894-3814.

ORCID ®

Yuanzhi Tang: 0000-0002-7741-8646

Notes

The authors declare no competing financial interest.

### ACKNOWLEDGMENTS

This work was supported by the National Science Foundation under Grants 1605692, 1710285, and 1739884. We acknowledge Dr. Ching-Hua Huang and Wenlong Zhang (Georgia Tech) for providing samples and related information. We thank beamline scientists Qing Ma (APS 5-BM-D), Sam Webb, Nicholas Edwards, Sharon Bone (SSRL BL 2-3), and Ryan Davis (SSRL BL 4-1) for help with synchrotron experimental setup and data collection. Portions of this study were conducted at the Advanced Photon Source (APS) and Stanford Synchrotron Radiation Lightsource (SSRL). APS is a U.S. Department of Energy (DOE) Office of Science User Facility operated for the DOE Office of Science by Argonne National Laboratory under Contract DE-AC02-06CH11357. Use of SSRL, SLAC National Accelerator Laboratory, is supported by the DOE Office of Science, Office of Basic Energy Sciences, under Contract DE-AC02-76SF00515.

#### REFERENCES

- (1) Van Gosen, B. S.; Verplanck, P. L.; Seal, R. R., II; Long, K. R.; Gambogi, J. Rare-earth elements; US Geological Survey, 2017.
- (2) Blissett, R.; Smalley, N.; Rowson, N. An investigation into six coal fly ashes from the United Kingdom and Poland to evaluate rare earth element content. *Fuel* **2014**, *119*, 236–239.
- (3) Long, K. R.; Van Gosen, B. S.; Foley, N. K.; Cordier, D. The principal rare earth element deposits of the United States: A summary

- of domestic deposits and a global perspective. In Non-Renewable Resource Issues; Springer, 2012; pp 131-155.
- (4) US Geological Survey. Mineral Commodity Summaries 2018; US Geological Survey, 2018; pp 132-133.
- (5) Park, D. M.; Brewer, A.; Reed, D. W.; Lammers, L. N.; Jiao, Y. Recovery of Rare Earth Elements from Low-Grade Feedstock Leachates Using Engineered Bacteria. *Environ. Sci. Technol.* **2017**, *51* (22), 13471–13480.
- (6) Maes, S.; Zhuang, W.-Q.; Rabaey, K.; Alvarez-Cohen, L.; Hennebel, T. Concomitant leaching and electrochemical extraction of rare earth elements from monazite. *Environ. Sci. Technol.* **2017**, *51* (3), 1654–1661.
- (7) Liang, Y.; Liu, Y.; Lin, R.; Guo, D.; Liao, C. Leaching of rare earth elements from waste lamp phosphor mixtures by reduced alkali fusion followed by acid leaching. *Hydrometallurgy* **2016**, *163*, 99–103.
- (8) Seredin, V. V.; Dai, S. Coal deposits as potential alternative sources for lanthanides and yttrium. *Int. J. Coal Geol.* **2012**, *94*, 67–93.
- (9) Franus, W.; Wiatros-Motyka, M. M.; Wdowin, M. Coal fly ash as a resource for rare earth elements. *Environ. Sci. Pollut. Res.* **2015**, 22 (12), 9464–9474.
- (10) Taggart, R. K.; Hower, J. C.; Dwyer, G. S.; Hsu-Kim, H. Trends in the rare earth element content of US-based coal combustion fly ashes. *Environ. Sci. Technol.* **2016**, *50* (11), 5919–5926.
- (11) Dai, S.; Finkelman, R. B. Coal as a promising source of critical elements: Progress and future prospects. *Int. J. Coal Geol.* **2018**, *186*, 155–164.
- (12) Blissett, R.; Rowson, N. A review of the multi-component utilisation of coal fly ash. *Fuel* **2012**, *97*, 1–23.
- (13) Seredin, V. V.; Finkelman, R. B. Metalliferous coals: a review of the main genetic and geochemical types. *Int. J. Coal Geol.* **2008**, 76 (4), 253–289.
- (14) Hower, J. C.; Groppo, J. G.; Joshi, P.; Dai, S.; Moecher, D. P.; Johnston, M. Location of cerium in coal-combustion fly ashes: implications for recovery of lanthanides. *Coal Combustion and Gasification Products* **2003**, *5*, 73–78.
- (15) Hood, M. M.; Taggart, R. K.; Smith, R. C.; Hsu-Kim, H.; Henke, K. R.; Graham, U.; Groppo, J. G.; Unrine, J. M.; Hower, J. C. Rare Earth Element Distribution in Fly Ash Derived from the Fire Clay Coal, Kentucky. *Coal Combust. Gasification Prod.* **2017**, *9*, 22–33
- (16) Kolker, A.; Scott, C.; Hower, J. C.; Vazquez, J. A.; Lopano, C. L.; Dai, S. Distribution of rare earth elements in coal combustion fly ash, determined by SHRIMP-RG ion microprobe. *Int. J. Coal Geol.* **2017**, *184*, 1–10.
- (17) Hower, J. C.; Qian, D.; Briot, N. J.; Henke, K. R.; Hood, M. M.; Taggart, R. K.; Hsu-Kim, H. Rare earth element associations in the Kentucky State University stoker ash. *Int. J. Coal Geol.* **2018**, *189*, 75–82.
- (18) Dai, S.; Zhao, L.; Hower, J. C.; Johnston, M. N.; Song, W.; Wang, P.; Zhang, S. Petrology, mineralogy, and chemistry of size-fractioned fly ash from the Jungar power plant, Inner Mongolia, China, with emphasis on the distribution of rare earth elements. *Energy Fuels* **2014**, 28 (2), 1502–1514.
- (19) Montross, S. N.; Verba, C. A.; Chan, H. L.; Lopano, C. Advanced characterization of rare earth element minerals in coal utilization byproducts using multimodal image analysis. *Int. J. Coal Geol.* **2018**, 195, 362–372.
- (20) Thompson, R. L.; Bank, T.; Montross, S.; Roth, E.; Howard, B.; Verba, C.; Granite, E. Analysis of rare earth elements in coal fly ash using laser ablation inductively coupled plasma mass spectrometry and scanning electron microscopy. *Spectrochim. Acta, Part B* **2018**, 143, 1–11.
- (21) Stuckman, M.; Lopano, C.; Granite, E. Distribution and speciation of rare earth elements in coal combustion by-products via synchrotron microscopy and spectroscopy. *Int. J. Coal Geol.* **2018**, 195, 125–138.
- (22) Taggart, R. K.; Rivera, N. A.; Levard, C.; Ambrosi, J.-P.; Borschneck, D.; Hower, J. C.; Hsu-Kim, H. Differences in bulk and

- microscale yttrium speciation in coal combustion fly ash. *Environmental Science: Processes & Impacts* **2018**, 20 (10), 1390–1403.
- (23) Laudal, D. A.; Benson, S. A.; Addleman, R. S.; Palo, D. Leaching behavior of rare earth elements in fort union lignite coals of North America. *Int. J. Coal Geol.* **2018**, *191*, 112–124.
- (24) Izquierdo, M.; Querol, X. Leaching behaviour of elements from coal combustion fly ash: an overview. *Int. J. Coal Geol.* **2012**, *94*, 54–66.
- (25) King, J. F.; Taggart, R. K.; Smith, R. C.; Hower, J. C.; Hsu-Kim, H. Aqueous acid and alkaline extraction of rare earth elements from coal combustion ash. *Int. J. Coal Geol.* **2018**, *195*, 75–83.
- (26) Cao, S.; Zhou, C.; Pan, J.-h.; Liu, C.; Tang, M.; Ji, W.; Hu, T.; Zhang, N. Study on influence factors of leaching of rare earth elements from coal fly ash. *Energy Fuels* **2018**, 32 (7), 8000–8005.
- (27) ASTM. ASTM C618-15, Standard Specification for Coal Fly Ash and Raw or Calcined Natural Pozzolan for Use in Concrete; ASTM International: West Conshohocken, PA, 2015. www.astm.org.
- (28) Renew, J. E.; Huang, C.-H.; Burns, S. E.; Carrasquillo, M.; Sun, W.; Ellison, K. M. Immobilization of heavy metals by solidification/stabilization of co-disposed flue gas desulfurization brine and coal fly ash. *Energy Fuels* **2016**, *30* (6), 5042–5051.
- (29) Yan, X.; Dai, S.; Graham, I. T.; He, X.; Shan, K.; Liu, X. Determination of Eu concentrations in coal, fly ash and sedimentary rocks using a cation exchange resin and inductively coupled plasma mass spectrometry (ICP-MS). *Int. J. Coal Geol.* **2018**, *191*, 152–156.
- (30) Tessier, A.; Campbell, P.; Bisson, M. Sequential extraction procedure for the speciation of particulate trace metals. *Anal. Chem.* **1979**, *51* (7), 844–851.
- (31) McLennan, S. M. Rare earth elements in sedimentary rocks; influence of provenance and sedimentary processes. *Reviews in Mineralogy and Geochemistry* **1989**, 21 (1), 169–200.
- (32) Dai, S.; Zhao, L.; Peng, S.; Chou, C.-L.; Wang, X.; Zhang, Y.; Li, D.; Sun, Y. Abundances and distribution of minerals and elements in high-alumina coal fly ash from the Jungar Power Plant, Inner Mongolia, China. *Int. J. Coal Geol.* **2010**, *81* (4), 320–332.
- (33) Hower, J. C.; Dai, S.; Seredin, V. V.; Zhao, L.; Kostova, I. J.; Silva, L. F.; Mardon, S.; Gurdal, G. A note on the occurrence of yttrium and rare earth elements in coal combustion products. *Coal Combustion and Gasification Products* **2013**, *5*, 39–47.
- (34) Hower, J. C.; Berti, D.; Hochella, M. F., Jr; Mardon, S. M. Rare earth minerals in a "no tonstein" section of the Dean (Fire Clay) coal, Knox County, Kentucky. *Int. J. Coal Geol.* **2018**, *193*, 73–86.
- (35) Parkhurst, D. L.; Appelo, C. Description of input and examples for PHREEQC version 3: a computer program for speciation, batchreaction, one-dimensional transport, and inverse geochemical calculations; US Geological Survey, 2013; pp 2328–7055.
- (36) Deady, É. A.; Mouchos, E.; Goodenough, K.; Williamson, B. J.; Wall, F. A review of the potential for rare-earth element resources from European red muds: examples from Seydişehir, Turkey and Parnassus-Giona, Greece. *Mineral. Mag.* **2016**, *80* (1), 43–61.
- (37) Ayora, C.; Macías, F.; Torres, E.; Lozano, A.; Carrero, S.; Nieto, J.-M.; Perez-Lopez, R.; Fernández-Martínez, A.; Castillo-Michel, H. Recovery of rare earth elements and yttrium from passive-remediation systems of acid mine drainage. *Environ. Sci. Technol.* **2016**, *50* (15), 8255–8262.
- (38) Takaya, Y.; Yasukawa, K.; Kawasaki, T.; Fujinaga, K.; Ohta, J.; Usui, Y.; Nakamura, K.; Kimura, J.-I.; Chang, Q.; Hamada, M. The tremendous potential of deep-sea mud as a source of rare-earth elements. *Sci. Rep.* **2018**, *8* (1), 5763.
- (39) Elliott, W. C.; Gardner, D. J.; Malla, P.; Riley, E. A new look at the occurrences of the rare-earth elements in the Georgia kaolins. *Clays and Clay Minerals* **2018**, *66* (3), 245–260.
- (40) Elzinga, E.; Reeder, R.; Withers, S.; Peale, R. E.; Mason, R.; Beck, K. M.; Hess, W. P. EXAFS study of rare-earth element coordination in calcite. *Geochim. Cosmochim. Acta* **2002**, *66* (16), 2875–2885.
- (41) Tanaka, K.; Takahashi, Y.; Shimizu, H. Local structure of Y and Ho in calcite and its relevance to Y fractionation from Ho in

- partitioning between calcite and aqueous solution. *Chem. Geol.* **2008**, 248 (1–2), 104–113.
- (42) Lin, R.; Stuckman, M.; Howard, B. H.; Bank, T. L.; Roth, E. A.; Macala, M. K.; Lopano, C.; Soong, Y.; Granite, E. J. Application of sequential extraction and hydrothermal treatment for characterization and enrichment of rare earth elements from coal fly ash. *Fuel* **2018**, 232, 124–133.
- (43) Lin, R.; Howard, B. H.; Roth, E. A.; Bank, T. L.; Granite, E. J.; Soong, Y. Enrichment of rare earth elements from coal and coal byproducts by physical separations. *Fuel* **2017**, *200*, 506–520.
- (44) Wood, S. A. The aqueous geochemistry of the rare-earth elements: Critical stability constants for complexes with simple carboxylic acids at 25° C and 1 bar and their application to nuclear waste management. *Eng. Geol.* **1993**, 34 (3–4), 229–259.